The Impact of Molecular Orientation on the Photovoltaic Properties of a Phthalocyanine/Fullerene Heterojunction

Barry P. Rand, David Cheyns, Karolien Vasseur, Noel C. Giebink, Sébastien Mothy, Yuanping Yi, Vaeceslav Coropceanu, David Beljonne, Jérôme Cornil, Jean-Luc Brédas, and Jan Genoe*

The anisotropy inherent to many planar organic molecules leads to a high sensitivity of various fundamental processes to the orientation of molecules within films and at heterojunctions. Such processes include absorption, charge and exciton transport, energy levels, and charge transfer, all of which are critical to organic solar cell operation. Here,an in-depth study of bilayer cells consisting of a donor/acceptor interface between zinc phthalocyanine (ZnPc) and fullerene (C_{60}) is conducted and devices with the typically deposited standing up (edge-on) orientation are compared to those with ZnPc lying flat (face-on). The face-on ZnPc-based device allows for an increase in all solar cell parameters, substantially increasing power conversion efficiency from 1.5% to 2.8%. Spectrally resolved photocurrent measurements reveal a >50% increase in ZnPc signal, from which only 12% is accounted for by the increase in absorption associated with the face-on orientation. The increase in internal quantum efficiency is accounted for via an improved charge transfer. The results of this study indicate that proper consideration of the orientation between donor and acceptor needs to be taken in order to fully optimize the numerous processes required for photovoltaic energy conversion.

1. Introduction

The considerable research effort focused on organic-based solar cells over the course of the last decade has allowed for the recent demonstration of power conversion efficiency (η_P) equal to 10%,[1] with the promise of continued rapid progress in the near future. Contributing to this progress has been research on new materials, thin film morphology, interface layers, device architecture, and fundamental understanding.[2] Of primary relevance to organic solar cell efficiency is the necessity to fulfill a series of subsequent processes in order for an incident photon to be converted into photocurrent. First, owing to the low dielectric constant and weak intermolecular electronic coupling characteristic of organic semiconductors, absorption leads to the creation of a Coulombically bound electron-hole pair, or exciton, whose binding energy can be on the order of 0.5 eV. Then, excitons must diffuse to a donor/acceptor (DA) interface where the exciton may dissociate, leaving behind an electron on the acceptor material, and a hole on the donor material. These two charges, however, remain Coulombically bound to one another in the form of a charge transfer (CT) state, which may either recombine to the ground state or subsequently dissociate into free charge carriers, overcoming the CT state binding energy through entropic increase aided by the internal electric field.[3] Finally, the charges must be transported from the DA interface to be collected at the electrodes. Therefore, to maximize device performance and the efficiency of these various processes, one would like to simultaneously optimize absorption strength, exciton diffusion length (L_D), charge transfer efficiency (η_{CT}), and charge carrier mobility.

As organic semiconducting thin films are made up of individual molecules held together by weak van der Waals forces, many of the physical properties of the solid are strongly influenced by the degree of intermolecular orbital overlap. In the case of planar or asymmetric molecules, and especially in crystalline materials, the implication is that transport of charges and excitons present some degree of anisotropy, aspects which have been experimentally verified.[4,5] Therefore, organic thin film transistors have benefitted from achieving vertical molecular alignment with molecules standing up, or edge-on, such that the π–π stacking direction is parallel to the substrate as well as the conducting channel.[6] Furthermore, optical properties such as absorption and emission are most often anisotropic, a

Dr. B. P. Rand, Dr. D. Cheyns, K. Vasseur, Dr. J. Genoe
imec, Kapeldreef 75, B-3001, Leuven, Belgium
E-mail: barry.rand@imec.be
Prof. N. C. Giebink
Department of Electrical Engineering
The Pennsylvania State University
University Park, PA 168002 USA
S. Mothy, Dr. D. Beljonne, Dr. J. Cornil
Laboratory for Chemistry of Novel Materials
University of Mons
Place du Parc 20, B-7000 Mons, Belgium
Dr. Y. Yi, Dr. V. Coropceanu, Prof. J. L. Brédas
School of Chemistry and Biochemistry
and Center for Organic Photonics and Electronics
Georgia Institute of Technology
Atlanta, GA 30332 USA

DOI: 10.1002/adfm.201200512

characteristic which has been exploited for both organic light emitting diodes[7] as well as for organic solar cells.[8] Finally, one should not neglect the change in energy levels that can be associated with a change in orientation of a thin film, and which can have an effect on heterojunction processes.[9]

Thus, for organic solar cell applications, it is beneficial to organize planar molecules within thin films comprising a face-on orientation. This is not only because charge and exciton transport should be improved in the vertical direction, but also owing to the larger absorption strength when the transition dipole moment of the planar molecule (typically along its long axis) is aligned with the electric field of the incident light. It was shown recently, via an annealing treatment, that a change in relative orientation of the molecules at the DA interface was responsible for a change in CT state energy that could impact the exciton dissociation probability.[10] Structural templating is another way to control molecular orientation, whereby molecules can adopt face-on rather than edge-on orientations depending on whether or not substrate-molecule interactions dominate molecule-molecule interactions.[11] This approach has been successfully applied multiple times for controlling the orientation or crystal phase of thin film growth for photovoltaic applications.[12,13]

Here, we employ a CuI template[14] to change the orientation of a zinc phthalocyanine (ZnPc) thin film from its normally edge-on orientation on an indium tin oxide (ITO) surface, to a face-on orientation. We first characterize the thin film morphological and optical properties of the ZnPc films. Then, when paired with C_{60} as an acceptor, we find an improvement in all photovoltaic performance parameters. We investigate the spectral response of the edge-on and face-on ZnPc-based devices, finding that the internal efficiency of ZnPc excitations is improved by 40% whereas that of the spherically symmetric C_{60} is unchanged. By systematically considering the various processes which are affected, including absorption and L_D, we find that while absorption is enhanced for face-on ZnPc, L_D is in fact reduced, even though the effective number of molecular planes over which an exciton can diffuse in the vertical direction is increased. We model the changes in the electronic coupling mediating at the quantum-chemical level, and find that the improved η_{CT} is able to account for the observed enhancement in photogeneration efficiency. Finally, transfer matrix-based simulations provide good agreement with the experimental and quantum-chemical findings. Overall, despite the many processes affected, it is possible to gain a better understanding of the effect of molecular orientation on DA-based organic solar cells.

2. Results

2.1. ZnPc Thin Film Properties

We first investigate the morphological and optical properties of ZnPc thin films in either the edge-on or face-on orientation. In order to confirm the orientation and templating effect of CuI, in **Figure 1** we plot the results of symmetric $\theta/2\theta$ X-ray diffraction (XRD) measurements which probe out-of-plane ordering.

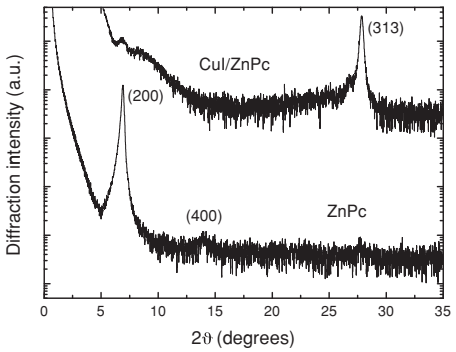

Figure 1. X-ray reflectivity of ZnPc(150 nm) (bottom curve) and CuI(1 nm)/ZnPc(150 nm) (top curve) on Si/SiO_2 substrates. The curves are offset vertically for clarity of presentation and the numbers in parentheses correspond to diffraction planes of α-phase ZnPc.

We use here a flat SiO_2 surface to increase the signal-to-noise ratio, while the templating effect on SiO_2 vs. ITO are assumed to be the same owing to similarly weak substrate-molecule interactions. For the ZnPc film, the foremost diffraction peak corresponds to a lattice spacing d = 12.8 Å and is assigned to α-phase (200), as the α–polymorph is known to form on non-interacting substrates at room temperature.[12] This means that crystallites are predominantly oriented with the ZnPc molecular plane perpendicular to the substrate surface, or in other words, in an edge-on orientation. Also visible is a weak second order diffraction peak, that of α-phase (400), suggesting a limited degree of long-range ordering. For ZnPc deposited on CuI, the situation is significantly different. The dominant diffraction peak emerges at 27.9°, but cannot unambiguously be assigned to the α–phase as the CuI interlayer is shown to influence the structure of the ZnPc layer. Besides the α–polymorph, another metastable thin-film polymorph is reported to exist in ZnPc films.[15,16] Despite different lattice symmetry, both polymorphs exhibit similar Bragg peaks which hampers phase identification. For both crystal structures however, the interplanar spacing of 3.2 Å indicates that the molecules adopt a face-on orientation on the CuI substrate. Also visible in the XRD measurement is a relatively weak feature at 6.9°, indicating that some crystallites continue to adopt the edge-on orientation, though the percentage of such crystallites within the film is assumed to be minimal.

It is known that the DA interface area is directly correlated to the photogenerated current, due to the increased probability for excitons to diffuse to a nearby interface.[17] Therefore, an increase in surface area of the $ZnPc/C_{60}$ DA interface could hamper the comparison of the two orientations should the templating lead to a significant difference in topography. In **Figure 2** we present atomic force microscope (AFM) scans of ZnPc films in either orientation, with a thickness of 17 nm, identical to that used in the device comparison of Section 2.2. The topography of the edge-on oriented ZnPc film deposited directly on ITO is shown in Figure 2a. The root mean square (rms) roughness of 4.9 nm is typical for polycrystalline phthalocyanine films, with a folding ratio (ratio of the surface area of the topographical image to a flat image) of 1.10. In comparison, the ZnPc film deposited on CuI (Figure 2b) possesses an rms roughness of 5.1 nm, with a

DOI: 10.1002/adfm.201200512

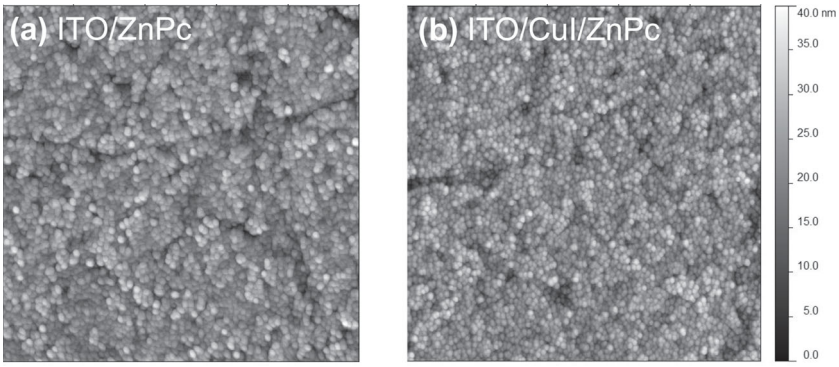

Figure 2. Topographic AFM images (2.5 µm × 2.5 µm) of 17 nm thick films of ZnPc (same thickness as those used in devices) on either a) ITO or b) ITO/CuI(1 nm).

folding ratio equal to 1.12. Both films are composed of nanoscale grains, an observation consistent with the fact that these films are polycrystalline. Analysis of the AFM images reveals an average grain size of 30 ± 5 nm. Overall, taking account of the rms roughness, folding ratio, and grain size, we conclude that the topography of either orientation is the same, and can therefore neglect the influence of surface roughness on the resulting solar cell performance comparison.

Finally, we compare the optical properties of ZnPc thin films in either the edge-on or face-on orientations. In **Figure 3**a we plot the complex optical constants $n + ik$ for 17 nm thick films as employed within devices. The refractive indices as well as the extinction coefficients reveal a significant enhancement for the ZnPc film deposited on CuI. These data are consistent with the fact that the oscillator strength for a given molecular transition is higher when the electric field of the incident light is aligned with the molecular dipole, the case for the face-on oriented ZnPc film. Also, these findings are similar to observations of anisotropic optical constants for planar molecules probed via variable angle spectroscopic ellipsometry.[18] This indicates significantly more absorption for normally incident light on the face-on ZnPc film compared to the edge-on film, the absorption lengths calculated from k being 36 and 50 nm at the peak Q-band absorption wavelength of λ = 620 nm, respectively. Finally, the peak Q-band wavelengths do not experience significant red-shifts, as would be the case for an α- to β-phase transition,[19] but a transition from α-phase to another metastable thin film polymorph cannot be rigorously excluded.

The emission spectra of edge-on ZnPc and face-on CuI/ZnPc films are shown in Figure 3b. In both cases, emission onsets for $\lambda \approx 750$ nm, just beyond the absorption edge of the films, and is quite broad, extending to $\lambda > 1000$ nm. While the edge-on ZnPc film has an emission peak at λ = 950 nm, the emission of the face-on film peaks at λ = 1025 nm. This longer wavelength emission does not originate from the CuI templating layer, as it neither absorbs at the excitation wavelength of λ_{ex} = 633 nm nor emits in this wavelength range. It is not clear whether there is a simple redistribution of emissive features, as we can clearly recognize the shoulder at λ = 950 nm for the face-on ZnPc film to be coincident with the emission maximum of the edge-on ZnPc film, or if the emissive feature at λ = 1025 nm originates from a new state. While we do not know the origin of the spectral differences, the long wavelength feature is excitonic in nature, and does not result from monomeric emission but rather from an aggregate excited state such as an excimer.[20]

2.2. Solar Cell Characterization

In order to probe the effect of molecular orientation of ZnPc on a solar cell, we fabricated planar heterojunction solar cells comprising a ZnPc/C_{60} DA interface. The edge-on ZnPc device has the following structure: ITO/ZnPc(17 nm)/C_{60}(40 nm)/bathocuproine (BCP; 10 nm)/Ag, whereas the face-on ZnPc solar cell has a 1 nm thick CuI layer between the ITO and ZnPc layers. In **Figure 4**, we plot the current density vs. voltage (J–V) characteristics under 1 sun (100 mW cm^{-2}) AM1.5G simulated solar illumination (Figure 4a) as well as in the dark (Figure 4b). By fitting the dark current to the generalized Shockley equation,[21] we can extract the diode parameters such as reverse saturation current density (J_0), ideality factor (n), series (R_s) and parallel resistances (R_p), as given in **Table 1**. The parameters reveal little

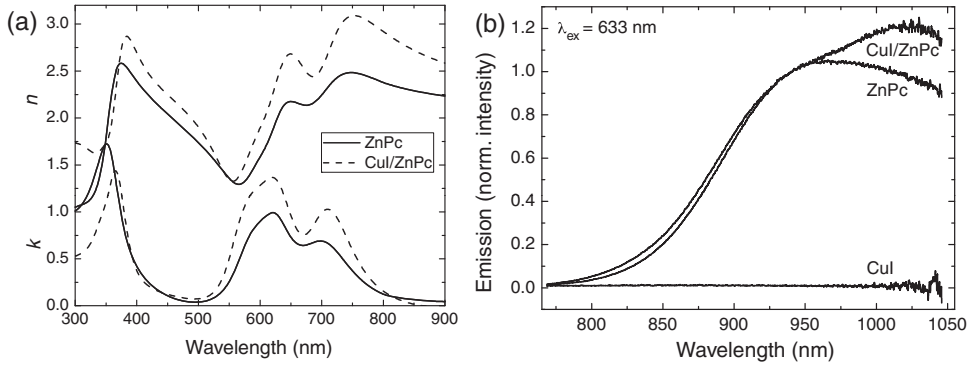

Figure 3. a) Measured complex refractive index $n + ik$ for thin films of ZnPc in the edge-on (solid curves) or face-on (dashed curves) orientation deposited on Si/SiO_2 substrates. b) Measured emission spectra on quartz for edge-on ZnPc(150 nm), face-on ZnPc(150 nm), and CuI(1 nm) under excitation at λ_{ex} = 633 nm.

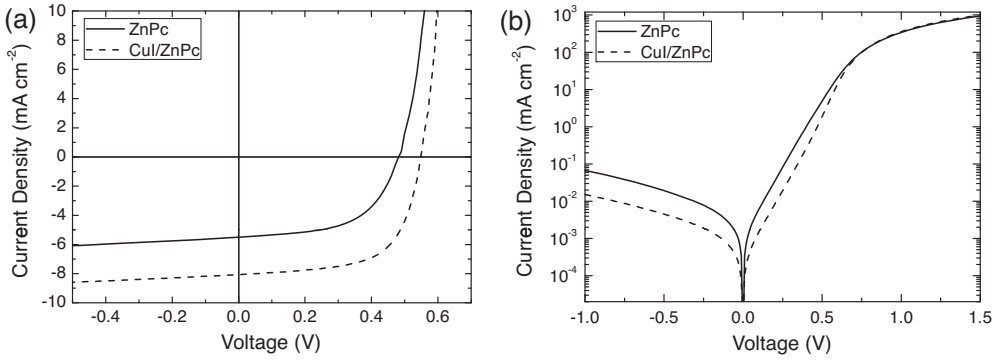

Figure 4. Measured current density vs. voltage characteristics for edge-on (solid curves) and face-on (dashed curves) ZnPc-based bilayer solar cells a) under 1 sun (100 mW cm^{-2}) AM1.5G simulated solar illumination and b) in the dark.

Table 1. Dark diode (J_0, n, R_s, R_p) and 1 sun illuminated solar cell performance parameters (J_{SC}, V_{OC}, FF, η_P, J_{EQE}) for ZnPc-based bilayer cells with edge-on or face-on orientations. J_{EQE} is the J_{SC} expected by integration of the EQE spectrum over the AM1.5G solar spectrum.

Device	J_0 [mA cm^{-2}]	n	R_s [Ω cm^2]	R_p [Ω cm^2]	J_{SC} [mA cm^{-2}]	V_{OC} [V]	FF [%]	η_P [%]	J_{EQE} [mA cm^{-2}]
ZnPc (edge-on)	1.3×10^{-6}	2.31	0.7	3.2×10^5	5.5	0.48	56	1.5	5.8
ZnPc (face-on)	7.7×10^{-8}	1.87	0.7	8.4×10^4	8.1	0.55	63	2.8	7.8

to no change in R_p and R_s, as a result of the change in ZnPc orientation, while J_0 and n are reduced in the face-on film. The lack of change in R_s suggests that the CuI layer does not have a deleterious effect on hole injection from the ITO anode, while the origins of the changes to J_0 and n remain unclear. This is in contrast to the two devices under illumination, where all of the photovoltaic performance parameters (cf. Table 1) present significantly different characteristics. It can be seen that the power conversion efficiency (η_p) is nearly doubled, from a value of 1.5% (edge-on) to 2.8% (face-on). The performance of the edge-on cell is in good agreement with previous studies,[22] whereas the face-on cell performance is noteworthy for a bilayer ZnPc/C_{60}-based solar cell. Contributing most to the increase in performance in going from edge-on to face-on is the nearly 50% increase in short-circuit current density (J_{SC}), which increases from 5.5 mA cm^{-2} to 8.1 mA cm^{-2} for edge-on and face-on ZnPc devices, respectively.

In an effort to better understand the reasons for the observed increase in J_{SC}, we conducted spectrally resolved measurements of the external quantum efficiency (EQE) as well as the total absorption efficiency (TAE; measured as 100% - reflection), the results of which are shown in **Figure 5**a. The TAE spectra reveal differences in absorption between the edge-on and face-on devices, including the effects of optical interference, and show an average increase of 12% throughout the ZnPc Q-band absorption range (550 nm < λ < 800 nm), whereas the absorption due to C_{60} was reduced by approximately 5% (400 nm < λ < 500 nm). This can be directly seen in the ratio of the edge-on to face-on spectra plotted in Figure 5b. The EQE spectra show a similar reduction in C_{60} signal corresponding to the 5% reduction in TAE, indicated by the fact that the calculated internal efficiency (EQE/TAE) plotted in Figure 5a is equal in the wavelength range attributed to C_{60} absorption. In the wavelength range corresponding to the ZnPc Q-band, we see that

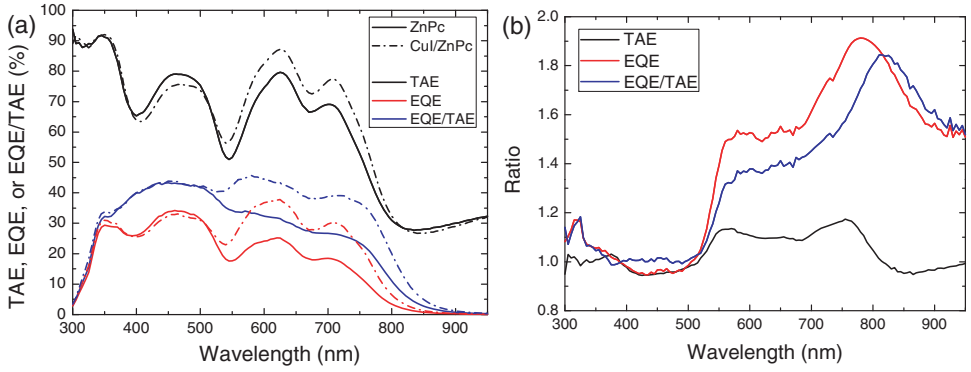

Figure 5. a) Measured total absorption efficiency (TAE; measured as 100% - reflection; black curves), external quantum efficiency (EQE; red curves), and the ratio EQE/TAE (blue curves) spectra for the edge-on (solid curves) and face-on (dash-dotted curves) ZnPc-based bilayer solar cells of Figure 4. b) The ratio of TAE (black), EQE (red), and EQE/TAE (blue), comparing face-on to edge-on ZnPc-based solar cells.

Adv. Funct. Mater. **2012**,
DOI: 10.1002/adfm.201200512

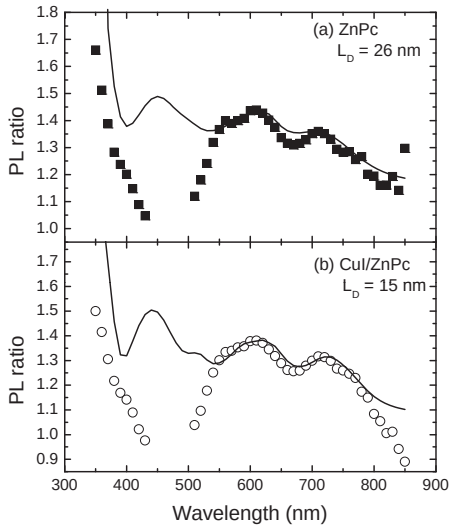

Figure 6. Photoluminescence (PL) excitation quenching ratio of the unquenched (150 nm thick film of ZnPc) to the quenched case (an additional 5 nm C_{60}) for a) edge-on and b) face-on ZnPc thin films. The solid lines show a transfer matrix model fit incorporating all thin film optical constants, and using the given exciton diffusion length (L_D).

EQE increases by a factor ≥50%. As this is measurably larger compared with the increase in TAE, there is a considerable increase (≥30%) in the internal efficiency of excitons originating from ZnPc, as shown in Figure 5a,b.

2.3. ZnPc Diffusion Length

One parameter that can have an influence on the EQE of ZnPc excitons is L_D, as it determines the volume of the ZnPc film over which photogenerated excitons are able to reach the DA interface. Owing to the weak but measurable emission of ZnPc (cf. Figure 3b), we can utilize a recently proposed technique for measuring L_D, that of spectrally resolved photoluminescence quenching (SR-PLQ).[23] Briefly, with SR-PLQ, we measure the photoluminescence excitation (PLE) spectrum of ZnPc either in the presence or absence of a quenching thin film, in this case a 5 nm thick film of C_{60}. We assume in the case of C_{60} as a quencher, that Förster energy transfer of ZnPc excitons to C_{60} is not possible owing to the negligible overlap of ZnPc emission with the absorption of C_{60}, and therefore that quenching is due entirely to excitons that are able to diffuse to the DA interface and undergo charge transfer. We then plot the ratio of the unquenched to the quenched PLE spectra, as shown in **Figure 6** for ZnPc either edge-on (Figure 6a) or face-on (Figure 6b). The data reveal a larger PL ratio in the case of edge-on ZnPc with respect to face-on ZnPc, indicative of a longer L_D for the edge-on ZnPc film. Transfer matrix simulations, utilizing the optical constants of ZnPc and C_{60}, were used in conjunction with the numerical solution of the one-dimensional diffusion equation to determine the steady-state exciton density profile throughout each layer (further details in the Experimental section). The integral of the exciton distribution is directly proportional to the emitted PL intensity, and hence the PL ratio can be calculated and fit to the data as shown in Figure 6, which yields $L_D = 26 \pm 2$ nm for the edge-on ZnPc film and $L_D = 15 \pm 2$ nm for the face-on ZnPc film. Note that the discrepancy in the spectral range 400–510 nm results from unavoidable collection of the excitation light grating double, rendering these points unreliable.

3. Discussion

The results of Qi *et al.* who used near-edge X-ray absorption fine structure spectroscopy to reveal the molecular tilt angle for edge-on and face-on α-phase copper phthalocyanine (CuPc) thin films,[24] combined with XRD results in Figure 1, allow us to propose schematics of the DA interface in the case of face-on or edge-on ZnPc, as shown in **Figure 7**. We should note that these representations portray a perfect situation, and not the real situation, where angular fluctuations occur, as exemplified by the AFM images in Figure 2 which reveal a ZnPc surface (and therefore the ZnPc/C_{60} interface) which is not perfectly flat. In the case of edge-on ZnPc, there is nominally a 64° angle between the ZnPc long-axis and the substrate plane, whereas the average tilting angle is reduced to 26° in the case of face-on ZnPc. For the latter film, we cannot unambiguously distinguish between a monoclinic and triclinic thin-film polymorph. In both cases, the observed Bragg peak at 27.9° corresponds to a stacking along the b-axis, which we schematically depicted in Figure 7b for a monoclinic herringbone stack. Furthermore, we can see a representation of the lattice plane spacing in the stacking direction as inferred from the diffraction peaks in Figure 1. Considering the edge-on ZnPc $L_D = 26 \pm 2$ nm, this corresponds to ≈20d, or 20 excitonic hops in the vertical stacking direction toward the DA interface. On the other hand, the face-on ZnPc film with $L_D = 15 \pm 2$ nm, translates to ≈47d. Then, given that $L_D = \sqrt{D\tau}$, where D is the exciton diffusivity and τ the exciton lifetime, and $D = \frac{1}{2}hd^2$,[25] where h is the one-dimensional hopping rate, yields

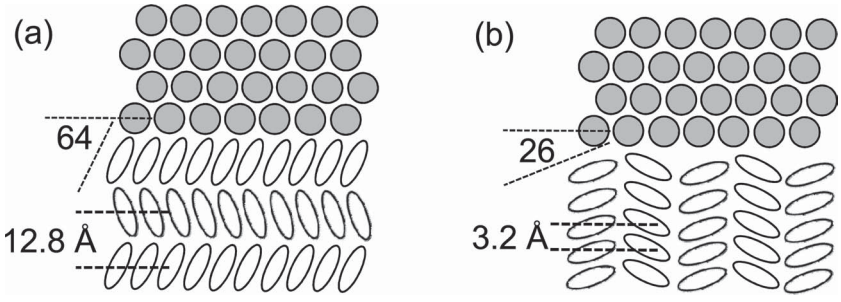

Figure 7. Schematics of the ZnPc/C_{60} heterojunctions for the cases of a) edge-on and b) face-on ZnPc orientations. ZnPc is represented by white ovals, whereas C_{60} is represented by grey circles. The expected angles between the ZnPc and C_{60} molecules are also given, as well as the lattice plane spacing in the stacking (growth) direction for the two orientations of ZnPc, as derived from the XRD results of Figure 1.

$$h = \frac{2L_D^2}{d^2\tau} \quad (1)$$

In our experiments, we did not detect any difference in τ depending on orientation. In both cases $\tau \approx 1.7 \pm 0.2$ ns, as determined by time-correlated single photon counting at several different emission wavelengths (data not shown). This means that h is increased by a factor of 5.3 for the face-on ZnPc film, which indicates that exciton transport in these ZnPc films, like absorption, is anisotropic, similar to that reported recently in rubrene.[5]

For proper consideration of η_{CT}, we conduct quantum-chemical simulations which have proven very useful to reveal fundamental processes at the DA interface.[26,27] In particular, we utilize a diabatic state approach based on an INDO/SCI description of the excitonic and charge-transfer electronic wavefunctions[28] to determine the effective electronic couplings, V_{eff}, for a ZnPc/C_{60} dimer as a function of rotational angle between ZnPc and C_{60} (cf. Figure 7). Using the Fermi Golden Rule, the rate for charge separation or recombination between diabatic states i and f goes as $k_{i\rightarrow f} = \frac{2\pi}{\hbar} V_{eff}^2 (i \rightarrow f)\rho\left(E_f\right)$, where the density of states $\rho(E_f)$ can be cast in terms of energy differences between the involved electronic states and reorganization energies associated with the electron transfer process as done in Marcus and related models.[27] It should be noted that, as opposed to what has been suggested previously,[10] preliminary Fourier-transform photocurrent spectroscopy spectra of the face-on and edge-on ZnPc/C_{60} devices (data not shown) do not reveal significant spectral differences, suggesting very similar CT state energies in the two cases. We thus focus here on the (squared) electronic couplings to gain a qualitative understanding of the effect of molecular orientation on the charge transfer processes. The values of V_{eff}^2 computed for charge recombination into the ground state and charge separation from either the excited ZnPc* or the C_{60}* molecule are shown in **Figure 8**. We distinguish two zones in the graph: from 15° to 35° corresponding to the face-on ZnPc thin film, and from 55° to 75° corresponding to the edge-on ZnPc case. In both zones, charge separation originating from excitation of the ZnPc molecule is more efficient than charge separation originating from excitation of the C_{60} molecule. In particular, we note that the angular dependence of the effective electronic coupling for charge separation from the C_{60}* molecule follows the same trend as for recombination. However, this trend is quite different compared to the case of charge separation from the ZnPc* molecule, which has an asymmetric profile.

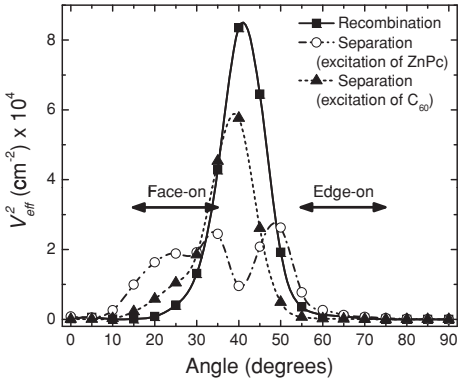

Figure 8. Calculated effective electronic coupling squared, V_{eff}^2, at the ZnPc/C_{60} heterojunction as a function of angle (cf. Figure 7) for the cases of charge separation of a ZnPc exciton (open circles, dash-dotted curve) or C_{60} exciton (filled triangles, dotted curve), as well as geminate electron-hole pair (CT state) recombination (filled squares, solid curve). Block arrows indicate the range of angles for face-on and edge-on configurations.

We can now comment on overall charge separation, which is dependent on the relative ratio of forward charge transfer and ground-state charge recombination between ZnPc and C_{60}. The fact that the ZnPc* separation follows a different trend compared to the other two cases suggests a larger orientational dependence for excitation into the ZnPc absorption band. Moreover, a larger electronic coupling is predicted around 30° for both charge separation cases, and we thus expect that the exciton dissociation will be favored in the face-on configuration due to a favorable overlap between molecular orbitals of ZnPc and C_{60}. The theoretical predictions confirm what we see directly in Figure 5b, where the ratio of the internal efficiency in the ZnPc absorption range is increased by ≥30%, while that corresponding to C_{60} excitation is unchanged (i.e., unity).

This improvement in η_{CT} is also reflected in the J–V characteristics of the devices under illumination, shown in Figure 4a, and, in particular, the increase in FF from 56% to 63%. An increased FF is an indication that the ability of a device to extract photocurrent has improved at voltage bias approaching V_{OC}, that is, when the external electric field that aids carrier extraction is considerably reduced with respect to short-circuit conditions. Considering the improvement in η_{CT} for ZnPc excitations in the face-on orientation, and the fact that ZnPc is responsible for a considerable majority of the photocurrent, we attribute the increase in FF to the increase in η_{CT}.

Another parameter that is improved in going from the edge-on to face-on device is V_{OC}, which increases from 0.48 V to 0.55 V under 1 sun illumination. As mentioned above, it does not appear that the presence of the CuI layer induces any extrinsic changes to the devices, and that the majority of the changes in dark and illuminated device performance are associated to the orientation change. One reason for the increase in V_{OC} could be due to the decrease (i.e. more negative) in highest occupied molecular orbital (HOMO) energy of the face-on film, which has been shown to be approximately 0.4 eV for CuPc thin films when comparing the two orientations.[29] This, together with the fact that the maximum V_{OC} of a DA pair is directly proportional to the donor HOMO level[21] (assuming they are paired with the same acceptor), can account for a larger V_{OC}. However, in this case, the data suggest that this only accounts for approximately half of the increase. The other half can be accounted for by the increase in J_{SC}, insomuch as an increased J_{SC} begets an increased V_{OC}, and by the reduction in dark saturation current (cf. Figure 4b and Table 1) for the face-on device, which follows from improved CT yield as expected from Figure 8.[30,31]

Utilizing transfer matrix-based simulations with the measured optical constants within the device structure as input, we can verify the observed changes in TAE comparing the edge-on to face-on-based ZnPc devices that were observed in Figure 5a.

Adv. Funct. Mater. 2012,
DOI: 10.1002/adfm.201200512

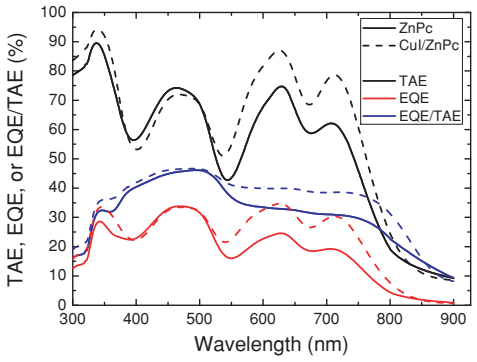

Figure 9. Simulated total absorption efficiency (TAE; black curves), external quantum efficiency (EQE; red curves), and the ratio EQE/TAE (blue curves) spectra for the edge-on (solid curves) and face-on (dashed curves) ZnPc-based bilayer solar cells of Figure 4.

The results of our simulations are plotted in **Figure 9**, and they show good agreement with the experimental TAE spectra, and aid in confirming two effects. The first is the observed increase in ZnPc absorption, which can be directly attributed to the increase in k in going from edge-on to face-on ZnPc (cf. Figure 3a). The second, and perhaps slightly less obvious effect, is the 5% reduction in C_{60} absorption when comparing the edge-on to face-on ZnPc-based devices, which is reproduced by the simulations and can be attributed to the increase in refractive index of ZnPc that alters the thin film interference effects within the structure and reduces the overall absorption in the C_{60} absorption range.

The TAE having been modeled, we can now simulate the EQE spectra of our solar cells. Using the L_D values for ZnPc as measured experimentally and the quantum chemical calculations as a guide for η_{CT} leaves us with only two fit parameters: L_D for C_{60} and η_{CT} for edge-on ZnPc*. We assume that once CT states are separated, the charge collection efficiency of these free charges is unity, a fair assumption for planar heterojunction devices. Furthermore, we assume that L_D for C_{60} is the same in the case of edge-on or face-on ZnPc, and fix the η_{CT} for C_{60}* as well as face-on ZnPc* to 100%, the latter of which may result in a slight overestimation of L_D. The simulated EQE and EQE/TAE spectra are plotted in Figure 9, and they reproduce quite accurately the experimental spectra in Figure 5a. We extract C_{60} $L_D = 19 \pm 1$ nm, in good agreement with previous values of our group with other donor materials.[32] The fitting for η_{CT} for edge-on ZnPc* yields a value of 75%, meaning that 25% fewer excitons are able to undergo charge separation in the case of edge-on ZnPc with respect to face-on ZnPc. This finding is in good agreement with the EQE/TAE ratio provided in Figure 5b, where one sees an enhancement of internal efficiency of ≥30% in the ZnPc-absorbing wavelength range.

4. Conclusions

We have analyzed the differences in photovoltaic performance of a ZnPc/C_{60} bilayer solar cell when the polycrystalline ZnPc layer has its orientation modified from the typical edge-on configuration to a face-on orientation. The templating in this case is achieved with a thin CuI layer, and its ability to induce a face-on orientation is confirmed with XRD measurements. Solar cells produced with the face-on and edge-on ZnPc films show a large increase in efficiency, from 1.5% to 2.8%, with increases in all performance parameters, most notably a substantial increase in J_{SC} and FF. Moreover, EQE measurements reveal that the increase in J_{SC} is due entirely to an increase in ZnPc photogeneration. The face-on ZnPc film presents an increased refractive index, which results in a ≈30% increase of absorption strength. Nevertheless, when incorporated within a thin film solar cell structure, due to optical interference effects the increase in absorption for the devices analyzed here is ≈12%. This points to an improvement in internal efficiency to allow for the majority of the J_{SC} gains.

We find that the excitonic hopping rate in the stacking (out-of-plane) direction is improved by more than five times in the face-on ZnPc film. However, owing to the lattice constant which is reduced by four times in going from an edge-on to a face-on film, the diffusion length of ZnPc excitons is in fact reduced from 26 ± 2 to 15 ± 2 nm. Via quantum-chemical calculations, we revealed that the effective electronic coupling for excited ZnPc* and C_{60}* charge transfer reactions possess different trends as a function of molecular tilt angle, and the ZnPc exciton dissociation follows a trend which is different from the C_{60} exciton as well as charge recombination, indicating that η_{CT} is improved for the face-on ZnPc film. Through this systematic analysis, and despite the many processes affected, we find a substantial opportunity for improving the performance of molecular-based solar cells by careful control of molecular orientation at the DA interface, and underscore the importance of analyzing the various mechanisms involved to enable a full optimization.

5. Experimental Section

Substrate Preparation and Thin Film Deposition: The substrates used in this study are glass substrates with 110 nm thick pre-patterned ITO (Kintec), highly doped n++-type silicon wafers with thermally grown SiO_2, and quartz substrates (AdValue Technology) for the SR-PLQ measurements. Substrate cleaning consisted of sonication in detergent, deionized water and acetone, followed by submersion in hot isopropanol. Finally, a 15 min ultraviolet-O_3 treatment was applied prior to deposition.

The organic materials, ZnPc (Sigma-Aldrich), C_{60} (SES research), and BCP (Sigma-Aldrich), were purified at least once using thermal gradient sublimation, while CuI and Ag were used as received. Organic thin films were deposited by thermal evaporation in a high vacuum evaporator with a base pressure $\approx 1 \times 10^{-7}$ Torr and growth rate of 1 Å s^{-1}, as monitored by a quartz crystal microbalance, and the substrate temperature was fixed to room temperature. Note: The thickness of ZnPc on CuI was systematically 70% of the thickness of ZnPc deposited on SiO_2, quartz, or ITO, as measured by ellipsometry, and was accounted for in the thicknesses deposited. For solar cell structures, subsequent layers were deposited in the same system without breaking vacuum. The Ag cathode is evaporated through a shadow mask, defining an active area of 0.134 cm^2.

Thin Film and Device Measurements: Optical constants are measured using spectroscopic ellipsometry (SOPRA, ges5). The regression was performed assuming an isotropic medium. Errors related to this assumption will be low, as ellipsometric measurements dominantly probe the optical properties out of plane, and the root-mean-square error after fitting was low. AFM images were collected using a Picoscan PicoSPM LE scanning probe operated in the tapping mode. The symmetric $\theta/2\theta$ XRD measurements were performed on a PANalytical

X´Pert Pro Materials Research Diffractometer using Cu Kα radiation. An integration time of 4 s was used for scanning 2θ in steps of 0.01°.

J–V characteristics of photovoltaic cells were measured in dark and under simulated solar light, using a Keithley 2602 in combination with an Abet solar simulator, calibrated to produce 100 mW cm^{-2} AM1.5G illumination. In the EQE and TAE setup, light from Xe and quartz halogen lamps were coupled into a monochromator and their intensities calibrated with a Si photodiode. The light incident on the device was chopped and the modulated current signal detected with current-voltage and lock-in amplifiers. TAE measurements were conducted with an integrating sphere.

For the SR-PLQ measurements, 150 nm thick ZnPc samples were excited at normal incidence through the front cover glass (films were encapsulated to prevent air exposure) with a bandwidth of approximately 5 nm. PL was detected at 30° from normal incidence on a CCD array in the wavelength range 910–960 nm and integrated to give the PL intensity for that excitation wavelength. Background intensity obtained from a blank substrate was subtracted to zero any offset. The PL ratio is the ZnPc only case divided by the (quenched) ZnPc/C_{60} case. Simulations were performed using transfer matrices to calculate the electric field intensity profile throughout the structure. This was taken as the initial excitation profile and was input to the diffusion equation,[33] which was solved numerically for the exciton density profile, the integral of which is proportional to the emitted PL intensity. Boundary conditions were assumed either perfectly quenching or non-quenching. These fits assume that the quartz and CuI interfaces are also quenching (i.e. only non-quenching interface is ZnPc/N_2).

Quantum-Chemical Calculations: The ground-state geometry of isolated ZnPc and C_{60} molecules has been optimized at the density functional theory (DFT) level using the B3LYP hybrid functional and the 6–V31g(d,p) basis set. The excited-state energies have been calculated using the intermediate neglect of differential overlap (INDO) method coupled to a single interaction configuration (SCI) technique.

The rotational angle is defined as the angle between the plane formed by the rotated ZnPc molecule and the plane formed by the ZnPc molecule in the lying-flat configuration. The ZnPc molecule is rotated while keeping approximately an intermolecular distance of 3.5 Å between the closest atoms within the ZnPc/C_{60} dimer.

The effective electronic coupling between the ground/excited (a) and charge transfer CT (b) states of the ZnPc/C_{60} dimer is defined as

$$V_{ab}^2 = \frac{1}{g}\sum_{ij}\left(\psi_{ai}\left|H\right|\psi_{bj}\right)^2$$

where g is the product of the degeneracy of involved states.

These calculations have been performed at the INDO level using the Mataga-Nishimoto potential. The CI active space is built by taking into account the π-type molecular orbitals for ZnPc (21 occupied and 19 unoccupied molecular orbitals) and C_{60} (30 occupied and 30 unoccupied molecular orbitals).

Spectral Response Modeling: The spectral response data is simulated using the transfer matrix formalism in order to extract L_D for C_{60} and η_{CT} for edge-on ZnPc*. After calculation of the optical interference pattern with these data, the generation of free carriers is calculated by solving a differential equation with L_D as parameter.[33] An exciton blocking boundary condition is used for the C_{60}/BCP interface, while an exciton quenching boundary condition is used at the ITO/ZnPc, CuI/ZnPc, and ZnPc/C_{60} interfaces, with only the latter producing photocurrent.

Acknowledgements

The authors acknowledge the FP7 European projects MINOTOR (NMP-228424) and ONE-P (NMP-212311) for financial support. The work in Mons is partly supported by the Interuniversity Attraction Pole IAP 6/27 of the Belgian Federal Government, and the Belgian Fund for Scientific Research (F.R.S.-FNRS/FRFC). K.V. acknowledges the Institute for the Promotion of Innovation through Science and Technology in Flanders (IWT-Vlaanderen) for financial support. S.M. is grateful to F.R.S.-FNRS for a doctoral fellowship. J.C. and D.B. are F.R.S.-FNRS Research Fellows. The work at the Georgia Institute of Technology is supported by the Office of Naval Research.

Received: February 21, 2012
Revised: March 27, 2012
Published online:

[1] M. A. Green, K. Emery, Y. Hishikawa, W. Warta, E. D. Dunlop, *Prog. Photovolt: Res. Appl.* **2012**, *20*, 12.
[2] a) C. J. Brabec, S. Gowrisanker, J. J. M. Halls, D. Laird, S. Jia, S. P. Williams, *Adv. Mater.* **2010**, *22*, 3839; b) R. Steim, F. R. Kogler, C. J. Brabec, *J. Mater. Chem.* **2010**, *20*, 2499; c) P. Heremans, D. Cheyns, B. P. Rand, *Acc. Chem. Res.* **2009**, *42*, 1740; d) A. W. Hains, Z. Liang, M. A. Woodhouse, B. A. Gregg, *Chem. Rev.* **2010**, *110*, 6689; e) B. C. Thompson, J. M. J. Frechet, *Angew. Chem. Int. Ed.* **2008**, *47*, 58; f) B. P. Rand, J. Genoe, P. Heremans, J. Poortmans, *Prog. Photovolt: Res. Appl.* **2007**, *15*, 659; g) J.-L. Brédas, J. E. Norton, J. Cornil, V. Coropceanu, *Acc. Chem. Res.* **2009**, *42*, 1691.
[3] C. Deibel, T. Strobel, V. Dyakonov, *Adv. Mater.* **2010**, *22*, 4097.
[4] V. C. Sundar, J. Zaumseil, V. Podzorov, E. Menard, R. L. Willett, T. Someya, M. E. Gershenson, J. A. Rogers, *Science.* **2004**, *303*, 1644.
[5] P. Irkhin, I. Biaggio, *Phys. Rev. Lett.* **2011**, *107*, 017402.
[6] a) M. M. Ling, Z. Bao, *Chem. Mater.* **2004**, *16*, 4824; b) H. N. Tsao, K. Müllen, *Chem. Soc. Rev.* **2010**, *39*, 2372.
[7] D. Yokoyama, *J. Mater. Chem.* **2011**, *21*, 19187.
[8] C. Videlot, A. El Kassmi, D. Fichou, *Sol. Energy Mater. Sol. Cells.* **2000**, *63*, 69.
[9] a) W. Chen, D.-C. Qi, H. Huang, X. Gao, A. T. S. Wee, *Adv. Funct. Mater.* **2011**, *21*, 410; b) G. Heimel, I. Salzmann, S. Duhm, N. Koch, *Chem. Mater.* **2011**, *23*, 359.
[10] A. Ojala, A. Petersen, A. Fuchs, R. Lovrincic, C. Pölking, J. Trollmann, J. Hwang, C. Lennartz, H. Reichelt, H. W. Höffken, A. Pucci, P. Erk, T. Kirchartz, F. Würthner, *Adv. Funct. Mater.* **2012**, *22*, 86.
[11] F. Schreiber, *Phys. Status Solidi (a)*. **2004**, *201*, 1037.
[12] P. Sullivan, T. S. Jones, A. J. Ferguson, S. Heutz, *Appl. Phys. Lett.* **2007**, *91*, 233114.
[13] a) T. Sakurai, R. Fukasawa, K. Saito, K. Akimoto, *Org. Electron.* **2007**, *8*, 702; b) B. E. Lassiter, R. R. Lunt, C. K. Renshaw, S. R. Forrest, *Opt. Express* **2010**, *18*, A444; c) B. Yu, L. Huang, H. Wang, D. Yan, *Adv. Mater.* **2010**, *22*, 1017; d) K. V. Chauhan, P. Sullivan, J. L. Yang, T. S. Jones, *J. Phys. Chem. C* **2010**, *14*, 3304; e) B. Verreet, R. Müller, B. P. Rand, K. Vasseur, P. Heremans, *Org. Electron.* **2011**, *12*, 2131.
[14] C. H. Cheng, J. Wang, G. T. Du, S. H. Shi, Z. J. Du, Z. Q. Fan, J. M. Bian, M. S. Wang, *Appl. Phys. Lett.* **2010**, *97*, 083305.
[15] P. Erk, H. Hengelsberg, M. F. Haddow, R. van Gelder, *Cryst. Eng. Commun.* **2004**, *6*, 474.
[16] C. Schuenemann, C. Elschner, A. A. Levin, M. Levichkova, K. Leo, M. Riede, *Thin Solid Films* **2011**, *519*, 3939.
[17] a) M. S. Kim, J. S. Kim, J. C. Cho, M. Shtein, L. J. Guo, J. Kim, *Appl. Phys. Lett.* **2007**, *90*, 123113; b) D. Cheyns, K. Vasseur, C. Rolin, J. Genoe, J. Poortmans, P. Heremans, *Nanotechnology* **2008**, *19*, 424016.
[18] D. Yokoyama, Z.Q. Wang, Y.-J. Pu, K. Kobayashi, J. Kido, Z. Hong, *Sol. Energy Mater. Sol. Cells.* **2012**, *98*, 472.
[19] L. Gaffo, M. R. Cordeiro, A. R. Freitas, W. C. Moreira, E. M. Girotto, V. Zucolotto, *J. Mater. Sci.* **2010**, *45*, 1366.
[20] K. Yoshino, M. Hikida, K. Tatsuno, K. Kaneto, Y. Inuishi, *J. Phys. Soc. Jpn.* **1973**, *34*, 441.

[21] B. P. Rand, D. P. Burk, S. R. Forrest, *Phys. Rev. B.* **2007**, *75*, 115327.
[22] a) Z. R. Hong, B. Maennig, R. Lessmann, M. Pfeiffer, K. Leo, P. Simon, *Appl. Phys. Lett.* **2007**, *90*, 203505; b) I. Bruder, J. Schöneboom, R. Dinnebier, A. Ojala, S. Schäfer, R. Sens, P. Erk, J. Weis, *Org. Electron.* **2010**, *11*, 377.
[23] K. J. Bergemann, S. R. Forrest, *Appl. Phys. Lett.* **2011**, *99*, 243303.
[24] D. Qi, J. Sun, X. Gao, L. Wang, S. Chen, K. P. Loh, A. T. S. Wee, *Langmuir* **2010**, *26*, 165.
[25] S. Chandrasekhar, *Rev. Mod. Phys.* **1943**, *15*, 1.
[26] a) Y. Yi, V. Coropceanu, J. L. Bredas, *J. Amer. Chem. Soc.* **2009**, *131*, 5131; b) D. Beljonne, J. Cornil, L. Muccioli, C. Zannoni, J.-L. Brédas, F. Castet, *Chem. Mater.* **2011**, *23*, 591; c) S. R. Yost, L.-P. Wang, T. Van Voorhis, *J. Phys. Chem. C* **2011**, *115*, 14431; d) Y. Yi, V. Coropceanu, J.-L. Brédas, *J. Mater. Chem.* **2011**, *21*, 1479; e) C. F. N. Marchiori, M. Koehler, *Synth. Met.* **2010**, *160*, 643.
[27] a) J.-L. Brédas, D. Beljonne, V. Coropceanu, J. Cornil, *Chem. Rev.* **2004**, *104*, 4971; b) V. Lemaur, M. Steel, D. Beljonne, J.-L. Brédas, J. Cornil, *J. Am. Chem. Soc.* **2005**, *127*, 6077.
[28] T. Kawatsu, V. Coropceanu, A. Ye, J.-L. Bredas, *J. Phys. Chem. C.* **2008**, *112*, 3429.
[29] W. Chen, H. Huang, S. Chen, Y. L. Huang, X. Y. Gao, A. T. S. Wee, *Chem. Mater.* **2008**, *20*, 7017.
[30] N. C. Giebink, G. P. Wiederrecht, M. R. Wasielewski, S. R. Forrest, *Phys. Rev. B* **2010**, *82*, 155305.
[31] It is very difficult to deconvolve the various processes contributing to V_{OC}, and to some extent the reduction in dark saturation current and HOMO level for face-on ZnPc disagree with the observation of no CT state energy change. This remains an open question beyond the scope of this work and will be the topic of a future study.
[32] D. Cheyns, B. P. Rand, P. Heremans, *Appl. Phys. Lett.* **2010**, *97*, 033301.
[33] L. A. A. Pettersson, L. S. Roman, O. Inganäs, *J. Appl. Phys.* **1999**, *86*, 487.